Theor. Comput. Fluid Dyn. (2006)
DOI 10.1007/s00162-006-0016-z

ORIGINAL ARTICLE

J.-Ph. Boin · J.-Ch. Robinet · Ch. Corre · H. Deniau

3D steady and unsteady bifurcations in a shock-wave/laminar boundary layer interaction: a numerical study

Received: 5 January 2005 / Accepted: 31 January 2006

Abstract The principal objective of this paper is to study some unsteady characteristics of an interaction between an incident oblique shock wave impinging a laminar boundary layer developing on a plate plane. More precisely, this paper shows that some unsteadiness, in particular the low frequency unsteadiness, originate in a supercritical Hopf bifurcation related to the dynamics of the separated boundary layer and not necessarily to the coherent structures resulting from the turbulent character of the boundary layer crossing the shock wave. Numerical computations of a shock-wave/laminar boundary-layer interaction (SWBLI) have been compared with a classical test case (Degrez test case) and both two-dimensional and three-dimensional (3D) unsteady Navier–Stokes equations are numerically solved with an implicit dual time stepping for the temporal algorithm and high order AUSM+ scheme for the spatial discretization. A parametric study on the oblique shock-wave angle has been performed to characterize the unsteady behaviour onset. Finally, discussions and assumptions are made about the origin of the 3D low frequency unsteadiness.

1 Introduction

Because of their ubiquitous presence in high-speed flight and their impact on vehicle and component performance, shock-wave/laminar boundary-layer interaction (SWBLI) have been studied for about 50 years. SWBLI occurs in an almost limitless number of external and internal flow problems and appears in many flow regimes (transonic, supersonic and hypersonic regimes). Despite remarkable progress in numerical simulation and experimental measurements, the characterization of the unsteady SWBLI remains a challenging issue. In order to understand these unsteady phenomena, some experiments have been provided for basic geometries like a purely supersonic boundary layer interaction on flat plate with an external shock generator. These studies yielded much useful data on the effects of Mach number, Reynolds number, and shock strength and reinforced the earlier observations of the importance of the state of the boundary layer.

Actually the interactions between a boundary layer (in turbulent regime or not) and a shock wave are not well understood. Initially, the studies focused on the comprehension of the properties of the initial boundary layer (in particular when it is turbulent) as it can act on the interaction and on the state of the downstream boundary layer. In the same way the strong distortion of the average field related to the shock can strongly contribute to the state of this downstream boundary layer. Lighthill's pioneer work, [1,2], on free interaction and self-induced separation has had a considerable influence on subsequent theoretical research on the SWBLI problem and in particular on the influence on the interaction of characteristic of the outer inviscid stream and the

Communicated by M.Y. Hussaini

J.-Ph. Boin · J.-Ch. Robinet (✉) · Ch. Corre
ENSAM/Paris SINUMEF Laboratory 151, Boulevard de l'Hôpital, 75013 Paris, France
E-mail: Jean-Christophe.Robinet@paris.ensam.fr

H. Deniau
LEA-CEAT, 43, route de l'aérodrôme, 86036 Poitiers Cedex, France

properties of the incoming boundary layer. However, there are another phenomena also being able to intervene in the interaction mechanisms, with rather different nature from those observed in the free interaction. They are dependent on instability mechanisms and can involve the SWBLI unsteadiness.

Two scenarios are opposed for the interpretation of the self-sustained low frequency oscillations: a first scenario is to seek the origin of the oscillations in the nature of turbulence in the boundary-layer, more precisely in the interaction of the upstream coherent structures with the shock. The second scenario does not seek the origin of the low frequency oscillations directly in the characteristics of turbulence but rather in the intrinsic dynamics of the separated zone, although in the second scenario the turbulence plays necessarily a part. Even if the boundary layer is laminar upstream, the boundary layer can become transitional in the interaction if the shock is strong enough. So the structure of the flow can be modified qualitatively. However, in this scenario, the low frequency dynamics of the shock/boundary layer system originates in the existence of intrinsic instabilities inside the separated zone almost independently of the turbulent nature of the boundary layer. It is within the framework of this second scenario that this article is.

The study of the interaction between a homogeneous and isotropic turbulence and a shock wave (Ribner [3], Kovasznay [4]) can help understanding such interaction mechanisms. This theory highlights the amplification of an isotropic homogeneous turbulence through a shock wave (the rapid distortion theory). In particular, when the Mach number is moderate (<5), the rotational mode is preponderant compared to the two other modes (entropic and acoustics modes), Morkovin [5]. Moreover, from an unsteady point of view, the addition of the signal generated by the oscillation of the shock can contribute to increase the level of fluctuation in the zone of excursion of the shock (Debieve and Lacharme [6]).

A review of the interaction modes putting forward the complexity of an oblique interaction between a shock wave and a boundary layer are proposed by Green [7] and more recently by Dolling [8]. When the incident shock is strong enough, the boundary layer becomes separated, thus generating a three-dimensional (3D) and unsteady recirculation zone. In this case, the rapid distortion theory does not take into account the totality of the amplification of the disturbances through shock (Smits and Muck [9]). The shock unsteadiness seems to play a part in this amplification. However, the origin of the shock unsteadiness itself is badly known, consequently several mechanisms are proposed to explain these oscillations. The turbulence of the boundary layer can cause displacements of the sonic line where the shock reflection occurs. In addition, the large structures of the external part of the boundary layer can be at the origin of the movements of the shock (Plotkin [10]). However, Thomas et al. [11] contradict this result: they show that there is no statistical link between the large structures of the incident boundary layer and shock oscillations. On the other hand, the pulsation of the separated zone is directly related to the oscillations of the shock. They propose to consider the shock and the separation bubble as a single dynamic system. Some authors have found that shock-induced separation of a turbulent boundary layer was characterized by a relatively low frequency compared to the incoming boundary-layer characteristic frequency (U_∞/δ) and a large scale pulsation. Dolling and Or [12] call upon an increase of the low frequency disturbances supported by the separation which contributes to thicken the subsonic part of the boundary layer. Selig and Smits [13] question the influence of the shock oscillations on the amplification of the disturbances. They propose to explain this amplification, by both an inviscid mechanism related to the strong distortion of the average field, and a mixture process on a large scale. This process should be controlled by instabilities in the external zone of the boundary layer and by longitudinal Taylor–Gœrtler instabilities in the vicinity of the separation and the reattachment points of the boundary layer.

In the present paper, another type of intrinsic instability related to the separated zone will be shown and this new instability is independent of the coherent structures related to the turbulent character of the flow. Therefore, the objective of this article is to show that the self-sustained low frequency oscillations in a SWBLI could originate in such instability. However, it is absolutely clear that the strictly laminar flow assumption is not correct when the incident shock angle is high because in more of the probable existence of a low frequency global instability, the boundary layer, when the angle of the incident shock angle is large, is convectively unstable and the boundary layer breakdown to turbulent state. Thereafter, convective instabilities will not be computed in order to clearly show the existence of a 3D global instability. The consequences of this assumption will be discussed thereafter.

The following article is divided into six sections: 1. The assumptions and the objectives of this work are specified in Sect. 2. The numerical method will be briefly described in sect. 3. Some validation cases of the numerical method used will be then proposed (Sect. 4). Results of two-dimensional (2D) and 3D computations are presented in sect. 5. In the next section the results are analyzed in details. Then we discuss the consequences of the assumptions made. Finally a scenario is proposed to explain the origin of low frequency unsteadiness (Sect. 6). In the last section prospects are given for future studies (Sect. 7).

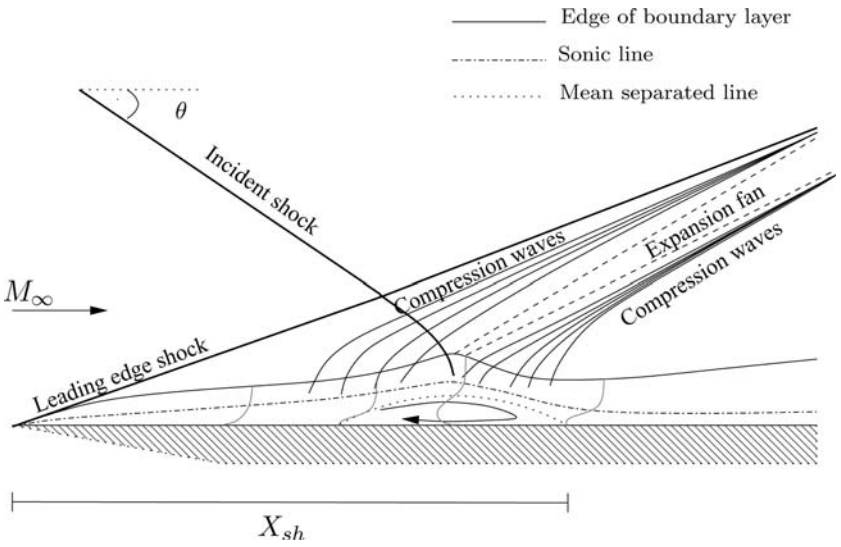

Fig. 1 Schematic representation of the shock wave/boundary layer interaction

2 Problematic and assumptions

The objective of this work is to demonstrate that the low frequency behaviour experimentally observed in SWBLI can be linked to the intrinsic dynamics of the detached zone induced by the interaction, independently of the turbulent boundary layer characteristics. To this end, the evolution of an incident shock wave impinging a laminar boundary layer developing over a flat plate when the incident shock angle is gradually increased has been studied, see Fig. 1. The freestream inflow Mach number and the global Reynolds number remain unchanged. The test case considered has been experimentally and numerically studied by Degrez et al.[14]. The freestream inflow Mach number is 2.15 for the numerical simulation. The Reynolds number based on the distance X_{sh} between the plate leading edge and the inviscid shock impingement point is 10^5. The shock angle with respect to the horizontal is initially equal to $\theta = 30.8°$, which corresponds to a shock generator angle of 3.75°. This dataset takes into account confinement, 3D effects and measurement approximations; it is not strictly the same as the experiment freestream conditions (see Degrez for more details).

At this incidence angle, Degrez et al. indicate that the flow remains stationary and 2D upstream, downstream and in the interaction. Furthermore it remains laminar at least until the end of the measurement zone. This configuration will be used to validate our numerical code.

The evolution of the SWBLI when the incident shock angle increases is a very complex problem. Indeed, for a particular value of the angle θ, the flow becomes transitional in the interaction zone. This transitional state will probably modify substantially the topology and the dynamics of the interaction zone. Although direct numerical simulations of laminar-turbulent transition of SWBLI are widely unreachable by current computer capacities, some computations can nevertheless be done under some assumptions. In this article, 2D and 3D computations will be done without taking into account the transitional character of the flow. Considering these assumptions, these present computations are meant to show that a SWBLI can become unsteady without taking into account the turbulent character of the flow. Then a scenario will be proposed where the unsteadiness onset are directly linked to the intrinsic dynamics of the detached zone leading quickly the flow to a 3D and unsteady system. Hypothesis as for the origin as of these unsteadiness will be formulated and a discussion about the consequences of the assumptions will be initiated.

3 Numerical methods

3.1 Space discretization

A numerical solution of the SWBLI is obtained by solving the 3D unsteady compressible Navier–Stokes equations written in conservative form:

$$\mathcal{U}_t + \left(f^E - f^V\right)_x + \left(g^E - g^V\right)_y + \left(h^E - h^V\right)_z = 0, \tag{1}$$

where $\mathcal{U} = (\rho, \rho u, \rho v, \rho w, \rho E)^T$ is the state vector expressed in terms of the conservative variables density, momentum and total energy, $f^E = f^E(\mathcal{U})$, $g^E = g^E(\mathcal{U})$ and $h^E = h^E(\mathcal{U})$ are the Euler fluxes, $f^V = f^V(\mathcal{U}, \mathcal{U}_x, \mathcal{U}_y, \mathcal{U}_z)$, $g^V = g^V(\mathcal{U}, \mathcal{U}_x, \mathcal{U}_y, \mathcal{U}_z)$ and $h^V = h^V(\mathcal{U}, \mathcal{U}_x, \mathcal{U}_y, \mathcal{U}_z)$ stand for the viscous fluxes in the three space directions. The system (1) is closed by assuming that the air satisfies the perfect gas state equation with a constant specific heats ratio equal to 1.4: $p = (\gamma - 1)\rho e$, with p the pressure and e the internal energy; moreover the Prandtl number is also supposed to be constant and set equal to 0.72. The system (1) is space-discretized on a Cartesian grid using the following conservative scheme:

$$\mathcal{U} + \frac{\left[\delta_1\left(\tilde{f}^E - \tilde{f}^V\right)\right]_{ijk}}{(\delta_1 x)_{ijk}} + \frac{\left[\delta_2\left(\tilde{g}^E - \tilde{g}^V\right)\right]_{ijk}}{(\delta_2 y)_{ijk}} + \frac{\left[\delta_3\left(\tilde{h}^E - \tilde{h}^V\right)\right]_{ijk}}{(\delta_3 z)_{ijk}} = 0, \tag{2}$$

where δ_p denotes the standard difference over a single grid cell in the pth space-direction, $\tilde{f}^E$, $\tilde{g}^E$ and $\tilde{h}^E$ are the numerical fluxes approximating the physical convective fluxes and $\tilde{f}^V$, $\tilde{g}^V$ and $\tilde{h}^V$ are second-order centered approximations of the physical viscous fluxes. The inviscid numerical fluxes are computed using the AUSM+ scheme developed by Liou & Edwards [15]. This scheme was retained over flux-vector splitting schemes such as Van Leer's for its well-known greater accuracy when applied to viscous flow computations and was also preferred over flux-difference splitting schemes such as Roe's for its reduced cost. Purely centered methods were ruled out for the present highly compressible flow calculations because they would have required the balance of artificial viscosity parameters and/or discontinuity sensors. High-accuracy of the inviscid numerical fluxes is ensured through the use of a fifth-order MUSCL reconstruction of the primitive variables vector $(\rho, u, v, w, p)^t$. Usually, the reconstruction process also involves the use of a slope limiter in order to avoid the numerical oscillations onset in the solution. The main effect of this limiting process is to bring down the accuracy of the scheme to the first order in flow regions where it is active: in turn, this reduction of accuracy can substantially alter the flow prediction, so that unsteady phenomena may no longer spontaneously appear. In the present study, the use of such limiter was not found necessary because enough natural dissipation is provided by the viscous terms to prevent the occurrence of numerical oscillations. For more details on the performances of this present solver with or without limiting process, see [16]. In addition, some comparisons were carried out between the present AUSM+ scheme used in this paper and a AUSMPW+ scheme [17,18]. This last scheme is a scheme which makes it possible to remove possible oscillations on the pressure close to a wall. In our configuration, the oscillations are quasi non existent with original AUSM+ scheme and no difference is observed.

3.2 Time integration

A time-accurate approximate solution of system (1) is obtained using the following implicit linear multi-step method:

$$\mathcal{T}\left(\mathcal{U}^{n+1}, \mathcal{U}^n, \mathcal{U}^{n-1}\right) + \mathcal{R}\left(\mathcal{U}^{n+1}\right) = 0, \tag{3}$$

where $\mathcal{R}$ gathers the space-discretization operators described in the previous section and $\mathcal{T}$ is a three-step approximation of $\mathcal{U}_t$ at time level $(n+1)$ defined by:

$$\mathcal{T}\left(\mathcal{U}^{n+1}, \mathcal{U}^n, \mathcal{U}^{n-1}\right) = (1+\phi)\frac{\left(\mathcal{U}^{n+1} - \mathcal{U}^n\right)}{\Delta t} - \phi\frac{\left(\mathcal{U}^n - \mathcal{U}^{n-1}\right)}{\Delta t} = (\mathcal{U})^{n+1} + \mathcal{O}\left(\Delta t^p\right). \tag{4}$$

The choice of $\phi = 1/2$ in formula (4) allows to reach second-order accuracy in time ($p = 2$). Although the order in time is not very high, the required global instabilities are generally low frequencies and the time step Δt of temporal advance is selected small around $\Delta t \sim 10^{-5}$ s. What is largely sufficient to compute required dynamics. In order to efficiently solve the implicit system $\mathcal{R}^\star\left(\mathcal{U}^{n+1}\right) = 0$ where $\mathcal{R}^\star\left(\mathcal{U}^{n+1}\right) = \mathcal{T}\left(\mathcal{U}^{n+1}, \mathcal{U}^n, \mathcal{U}^{n-1}\right) + \mathcal{R}\left(\mathcal{U}^{n+1}\right)$, one makes use of a dual time technique, well known for incompressible flow calculations [19] and made popular by Jameson [20] for computing compressible flows. Actually, $\mathcal{U}^{n+1}$ is obtained as a steady solution of an evolution problem with respect to a dual or fictitious time τ:

$$\mathcal{U}_\tau + \mathcal{R}^\star(\mathcal{U}) = 0. \tag{5}$$

Solving (5) instead of (3) allows the use of much larger physical time-steps; however, in the meantime, it also requires converging to a pseudo steady state at each physical time-step. Therefore, the dual time approach is of interest only if system (5) can be efficiently solved. In the present study, a matrix-free point-relaxation method allows to obtain a steady solution of system (5) after a few number of sub-iterations on the dual time (here around 200); moreover this implicit treatment induces a low memory storage requirement which makes the treatment of a large number of grid points accessible with moderate computer configurations (see for instance Luo et al. [21] for more details on this implicit technique).

3.3 Computational domain and boundary conditions

The numerical method described in the previous sections is applied to the computation of an oblique SWBLI on a flat plate. Experimentally, the oblique shockwave is generated using a wedge which deflects the incoming supersonic flow; numerically, it is sufficient to impose the incoming supersonic flow $V_\infty = (\rho_\infty, u_\infty, v_\infty, w_\infty, p_\infty)^T$ on the lower part of the inlet plane $x = 0$ (see Fig. 2a) while another (supersonic) state V_{down} is imposed on the upper part of the inlet plane and on the top plane ($y = y_{\max}$): this state is computed so as to satisfy the Rankine–Hugoniot relations across a shock with the upstream state V_∞ and given shockwave angle θ. The oblique shockwave begins on the inlet plane and propagates through the domain down to the flat plate (see Fig. 2a). At the exit plane, the conservative variables are extrapolated at the first-order from the values at the nearest upstream location; note this extrapolation is well posed for the supersonic inviscid flow outside the boundary layer but also for the subsonic flow in the boundary layer close to the wall because of the parabolic nature of the flow equations in this region. The flat-plate is assumed to be an adiabatic wall where velocity

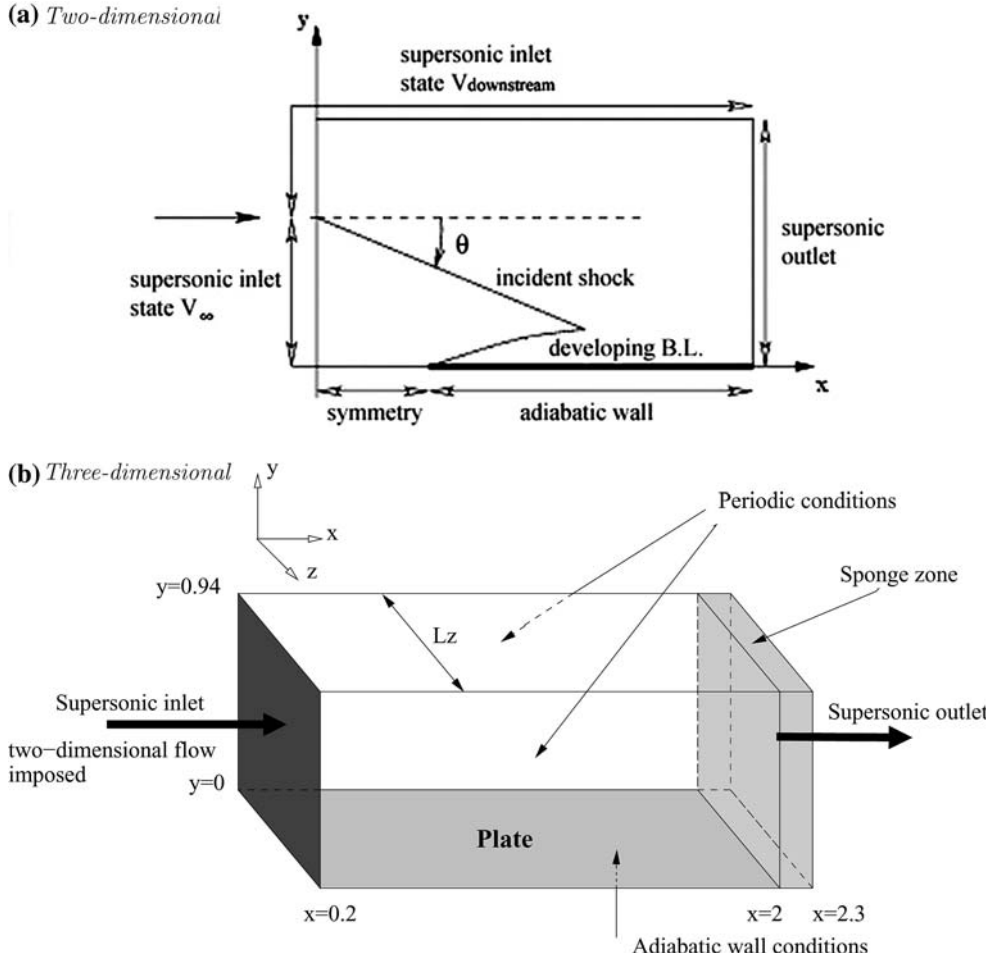

Fig. 2 Computational domain and boundary conditions. **(a)** Two-dimensional (2D), **(b)** Three-dimensional (3D)

vector is zero (no-slip condition); pressure is extrapolated at first-order from the values just above the plate. A symmetry condition is imposed along the line $y = 0$ upstream of the flat plate.

For 3D computations, the above conditions are extended along the z direction while periodic boundary conditions are used on the lateral planes. These boundary conditions are classically used in direct numerical simulation but will have important consequences on the results analyzed in this study. Indeed, in the case of a flow that naturally produces 3D structures, the dimension L_z given to the domain in the z-direction will force the wavelength of the transversal structures. Therefore, the transversal dimension should ideally be as large as possible to let 3D instabilities appear spontaneously. For DNS study of convective instabilities, L_z is fixed and corresponds to the most unstable wavelength, which appears first and is representative of the real configuration (without lateral boundaries). This wavelength is generally short comparing to the other characteristic dimensions of the problem and is given by a linear stability calculation. The present SWBLI study is focused on low frequency phenomena with corresponding large wavelengths; moreover there is no way to determine in a reliable way the wavelength of the strongest instability in that case. It was therefore decided to consider L_z as a parameter rather than a fixed input data; for all the 3D computations a parametric study on L_z is needed.

4 Preliminary computations

The first step is to compute the Degrez test case in order to validate our numerical simulation. The computational domain coordinates are non-dimensioned by the interaction length X_{sh}. The 2D domain extends from $x = -0.18$ to $x = 2$ and from $y = 0$ to $y = 0.94$ meshed with 600×180 points. The 3D domain is more restricted than 2D domain for x direction: $x = 0.2$ to $x = 2$, and the same in y direction but with 400×180 points. The spanwise length L_z lies between 0.1 and 3 with a number of plans ranging between 40 and 60 plans. The 3D dimensionless mesh spacing is equal to $\Delta x = 4.5 \times 10^{-3}$, $\Delta y = 7.8 \times 10^{-5}$ at the wall and from $\Delta z = 1.05 \times 10^{-3}$ to $\Delta z = 5 \times 10^{-2}$. The boundary layer profile, issued from 2D computation is imposed at location $x = 0.2$ and a sponge zone is imposed from $x = 2$ to $x = 2.3$. The dual CFL number is 50 and the convergence for the dual iterations is obtained after the residual decreases of 6 orders. The dimensional physical time step is equal to $\Delta t = 6.82 \times 10^{-6}$s that gives a physical CFL number close to 6.

For the Degrez test case ($\theta = 30.8°$), the 3D computed flow is not dependent to the spanwise direction; it is rigorously 2D and stationary like the one observed in the experiment. The pressure distribution, normalized by minimum pressure p_0 just upstream of the interaction and the skin-friction distribution along the plate are displayed in Fig. 3. 2D and 3D computations are very close to the experimental results, especially in the separated zone. One of the most sensible characteristics of the stream is the location of this detached zone. The computations give an accurate prediction of both the detachment point D and the reattachment point R, the latter being generally more difficult to obtain.

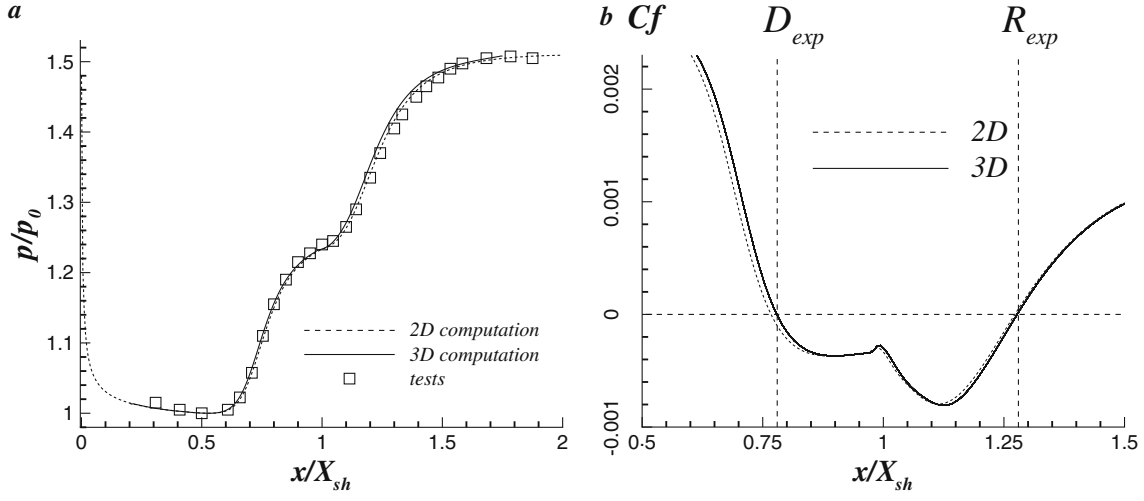

Fig. 3 Shock/boundary layer interaction. Pressure **(a)** and skin-friction distribution **(b)** along the plate

5 Parametrical study on incident shock angle

The objective is to study the unsteady flows onset in the case of a SWBLI and to describe the topology and the temporal dynamic inside and outside the interaction. The incident shock angle is increased without changing the shock impingement point. In this condition, the Reynolds number remains the same. The objective is to show that a self-sustained low frequency unsteady state can be reached in a fully laminar flow. The description of the whole complex flow is not in our purpose. Several major simplifications have been made. The first and probably the most important one is that we don't take into account the transition to a turbulent regime when the incident shock angle increases (see Sect. 1.).

5.1 Second preliminary computations: 2D case

For 2D computations we use the same domain as the one described previously. The increasing of the incident angle θ does not induce, at the beginning, any topological modification compared to the reference case (Degrez test case). But when we reach an angle of 32.5°, the emergence of a secondary detached zone inside the bulb close to the wall is observed, then the onset of secondary vortex close to the downstream mixing layer inside the main recirculation zone, Fig. 4a–c. This change arises for an angle included between 32.6° and 32.7°. The skin-friction coefficient becomes positive in the central zone of the bulb. When the angle is increased, the global size of the bulb and the size of the secondary detached zone grow considerably. Nevertheless for all angles considered here ($\theta \in [30.8°, 35°]$), the flow remains stationary. It is important to note that when the incident shock angle increases, some vortices appear near the shear layer downstream to the interaction

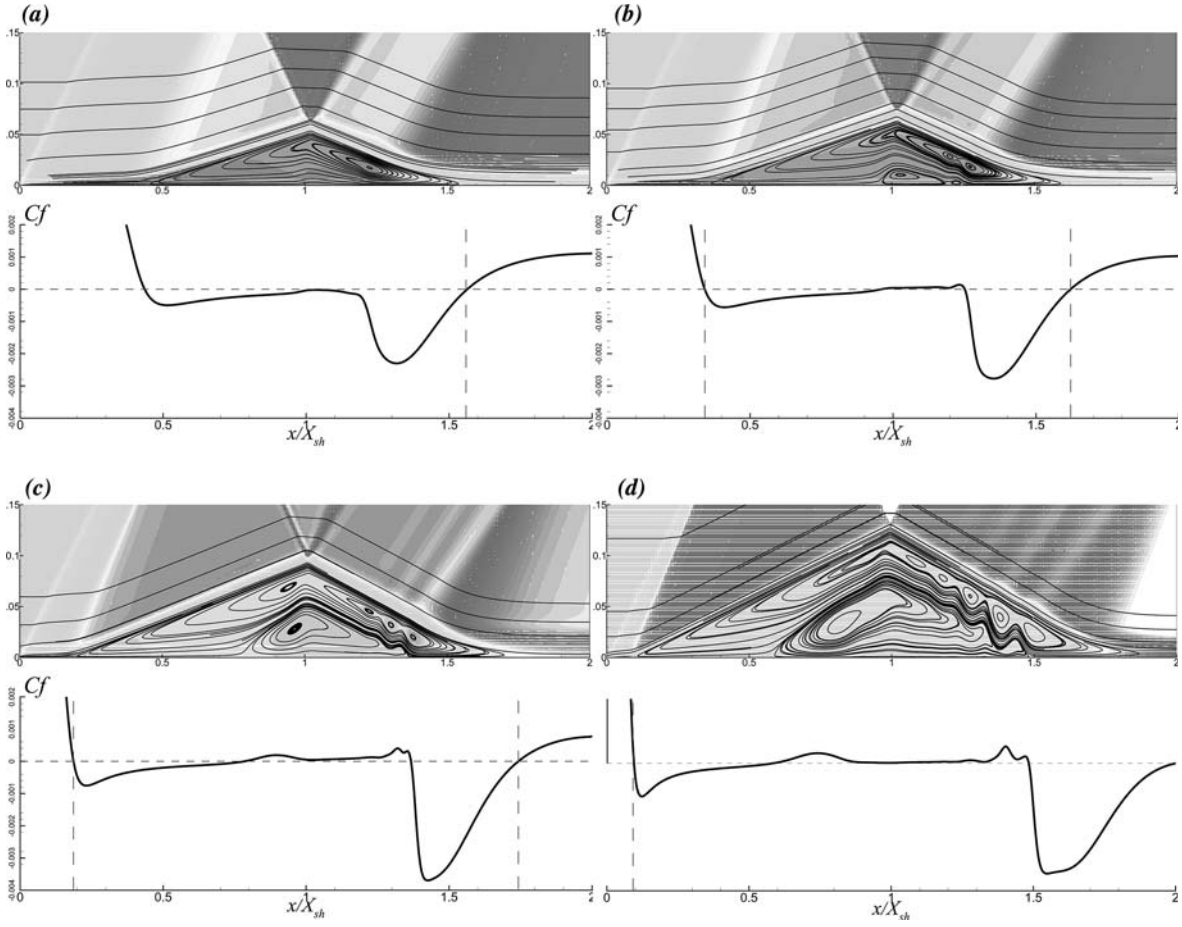

Fig. 4 Isochors and streamlines, skin-friction coefficient for $\theta = 32.5°$ **(a)**, 33° **(b)**, $\theta = 34°$ **(c)** and 35° **(d)** vertical to longitudinal ratio is 3.5

point. This characteristic seems to be linked to the 2D computation and as we shall see below it does not exist in the 3D computations. That can be interpreted like a lake mixture of the fluid characteristic of the 2D flows. This unphysical fragmentation of the internal zone of the recirculation bubble when the incident angle increases involves, for angles greater than 34° and the sensitivity to different numerical parameters like the mesh, the parietal boundary conditions and the initial conditions of computation is also observed. The size of the separated zone, in particular the reattachment point becomes difficult to define with precision. Moreover, for some grids, in particularly when the y direction is geometric, the dynamics of the flow can become unsteady. This spurious unsteady characteristic is directly related to the internal topology of the separated zone and more precisely of the number of secondary recirculations. In order to specify this mesh sensitivity for the case $\theta = 35°$, a computation with a uniform grid in x ($\Delta x = 3.34 \times 10^{-3}$), uniform in y when $y/X_{sh} < 0.15$ ($\Delta y = 4.34 \times 10^{-4}$) and geometrical grid with a reason equal to 1.02 when $0.15 < y/X_{sh} < 0.94$ with 620×600 points. Figure 4d illustrates this computation. In this grid, the convergence is reached. SWBLI is stationary for $\theta = 35°$. Different computations have been provided with some numerical schemes (WENO 3 and 5, OSMP 7, AUSM+ 3, 5 and 7), all these schemes in this grid give the same result (for more detail for this computational case see Robinet et al. [22]).

5.2 3D computations

In order to describe accurately the intrinsic bifurcation of the flow toward a 3D configuration without any geometric dependencies; the third direction is assumed to be unlimited. Periodic boundary conditions are imposed in the z-direction.

5.2.1 Introduction

The introduction of the third direction puts indeed the problem of computation capacities but also in the choice of the spanwise length L_z. This domain is initialized by a boundary layer profile which is previously computed at $x = 0.2$ in the 2D configuration. The 3D computational domain is described in Sect. 3.3 and it is summarized on Fig. 2b. The objective of this section is to characterize the spontaneous onset of the three-dimensional instabilities according to two parameters: incident shock angle θ and spanwise wavelength L_z. To limit the number of cases, two axes have been shown here. Firstly, the incident shock angle is constant and equal to 32°. In this case, only the spanwise L_z is modified. Under these conditions, a sample representative of the physics of a 3D interaction should be observed. Computations have been realized with a spanwise L_z varying from 0.1 to 3 but only few cases are presented here. Secondly, only the incident shock angle varies from 31.5^o to 32.5° with a constant spanwise L_z equal to 0.8. However, the whole of the treated cases is synthesized on the Fig. 17. When $\theta = 30.8°$, the flow is already known to be 2D and stationary (see Sect. 4). The first 3D computations have shown that when L_z is of the order of the interaction length X_{sh}, the 3D character is the most important. Beyond, the observed structures repeat as often as the transversal dimension allows it. The bifurcations from the steady 2D flow to the steady 3D flow and an unsteady 3D case will now be studied in details.

5.2.2 3D bifurcations

The incident shock angle is fixed at $\theta = 32°$. When the transverse dimension is smaller than 0.2 times the interaction length X_{sh}, the flow is still two-dimensional and stationary. When $L_z = 0.2$, the first bifurcation observed is a steady 3D one. Figure 5a shows a surface streamlines visualization on the plate for $L_z = 0.2$ (flow coming from the left). The freestream are quasi-parallels and the separation and reattachment lines on the plate are 2D and perpendicular to the freestream. Figure 6b shows a 3D view from the inside of the bulb. The surface streamlines appear on the plan $y = 0$ and on a median plan $z =$ constant. The streamlines are represented in 3D by ribbons of which the color is a function of the transverse velocity amplitude $| w |$. Even for $L_z = 0.2$, the 3D character appears spontaneously, but the transverse velocity amplitude remains weak (10^{-3}). For a larger spanwise length L_z, the amplitude of w is the same order as u or v inside the separated zone. Results are presented in Figs. 5b and 6b for a spanwise L_z equal to 0.4. The separation line is slightly curved whereas the reattachment line undergoes a strong deformation. In this case, the envelope of the bubble is strongly modulated in the third direction. The 3D character occurs also inside the recirculation zone with the existence of two counter rotating vortex tubes in which some fluids from the wall is transported to the

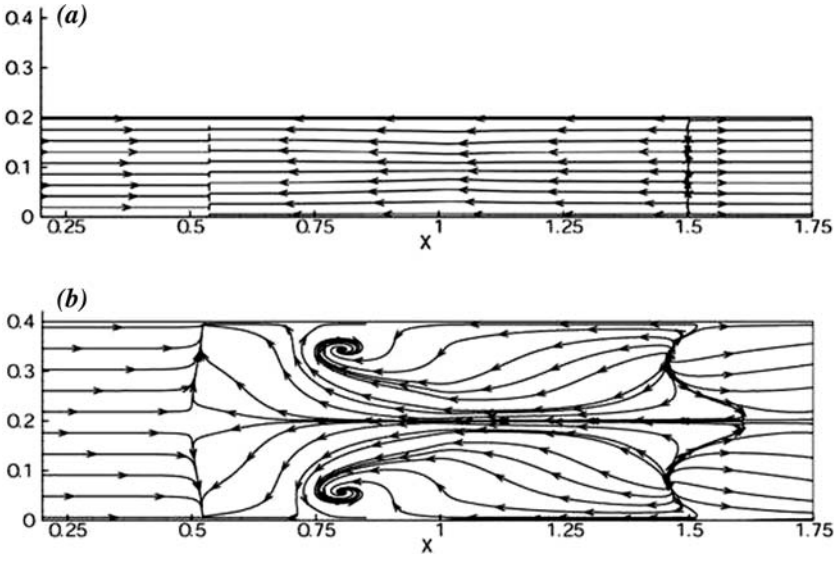

Fig. 5 Surface streamlines on the plate, $L_z = 0.2$ **(a)**, $L_z = 0.4$ **(b)**, $\theta = 32°$

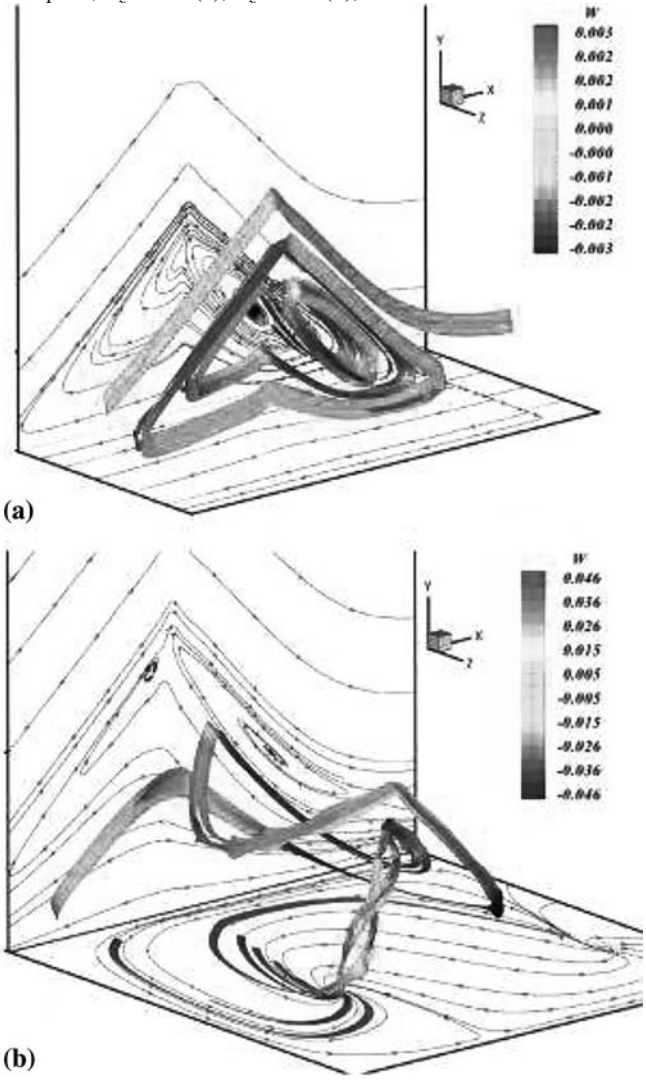

Fig. 6 3-Dimensional view inside the bulb, $L_z = 0.2$ **(a)**, $L_z = 0.4$ **(b)**, $\theta = 32°$

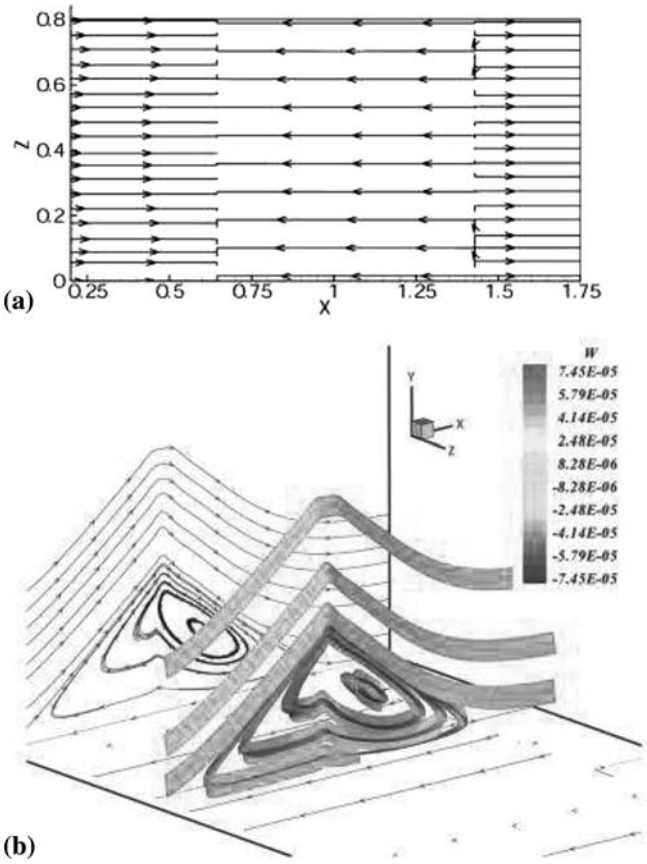

Fig. 7 Surface streamlines and 3D view, $L_z = 0.8$, $\theta = 31.5°$

downstream shear layer. For a greater spanwise length, $L_z = 0.8$ (in fact for $L_z \geq 0.6$), the flow becomes highly 3D and unsteady. This particular case is detailed in the following section.

Spanwise length L_z is now fixed equal to 0.8 and the incident shock angle varies from $\theta = 30.8°$ to $\theta = 33°$. Up to 31.7°, the flow remains 2D and stationary (Fig. 7). When the angle increases, the flow is destabilized. At 32°, it is fully 3D and unsteady. When the scanning between these two values is done, no stable 3D and stationary configuration is found. In order to characterize of the Hopf bifurcation, an amplitude parameter is defined as $A_{mp} = \max(w(t)) - \min(w(t))$, where $\max(w(t))$ and $\min(w(t))$ are the maximum and the minimum of $w(t)$, respectively. Fig. 8 shows the amplitude of the oscillations of w in a particular point in the SWBLI for the established flow and for $L_z = 0.8$. The characteristics of the supercritical Hopf bifurcation are observed. In order to characterize with more details the flow dynamics, some pressure spectra were calculated in certain point of the flow. The Fig. 9 show some temporal evolutions of pressure for different point in the flow: (a) is located in the inviscid zone and outside the SWBLI, (b) is located outside the boundary layer and near the reflected shock wave, (c) is located outside the boundary layer and near the interaction zone between the incident shock wave and the boundary layer, (d) is located inside the separated zone, near the shear layer. Figure 10 show the pressure spectra density for these different points. Strongly nonlinear temporal dynamics is mainly dominated by a fundamental frequency around 700 Hz, the secondary frequency activity results from the harmonics of this fundamental frequency. The nonlinear character of dynamics is rather important because $\theta = 32.5°$ is already sufficiently far away from the critical angle $\theta_c \simeq 31.7$. For $\theta = 32°$ the nonlinear dynamics is less important. A study on the dependence of the Hopf bifurcation with respect to the grid was undertaken for $L_z = 0.8$, this type of phenomenon being generally strongly depend on the grid. Table 1 gives the evolution of the critical angle θ_c and the frequency according to the grid. For the grid usually used, a small dependence on the grid is observed but this one remains acceptable. The Hopf bifurcation is thus qualitatively captured with the grid (400×180) even if in this grid it is still slightly numerically dependent on the grid.

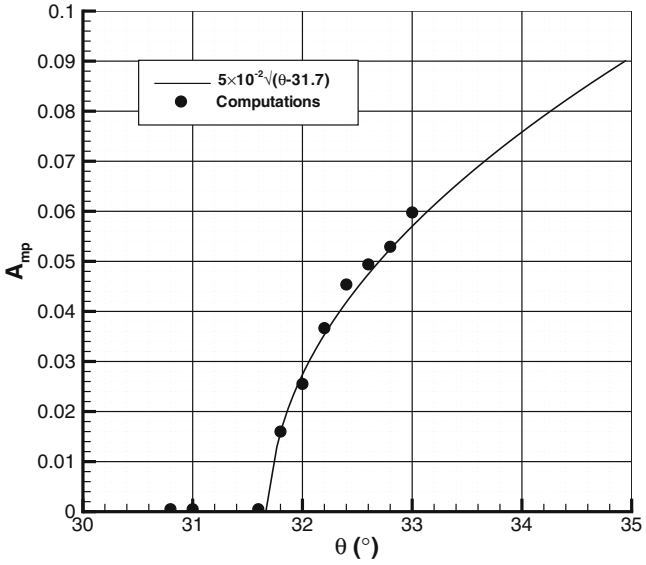

Fig. 8 The amplitude of the oscillations of w as a function of θ. • Numerical simulations, line : $A_{mp} \sim \sqrt{\theta - 31.7}$ at $(x_0, y_0, z_0) = (1, 5 \times 10^{-2}, 0.4)$, $L_z = 0.8$

However this grid is used for the whole of computations because a finer grid would have been prohibitory. It is however clear that so that this bifurcation can be regarded as physically established, it is necessary to carry out numerical simulations with other numerical schemes, in particular of the schemes which minimize and control the numerical dissipation.

Finally, when the spanwise length $L_z \geq 0.8$, several instabilities with different transverse wavelengths can coexist, it is not possible to isolate a particular wavelength. The study of the transient phase of the unsteady 3D case $\theta = 32°$, $L_z = 0.8$, is going to give us more information about the coexistence of the different 3D instabilities.

Table 1 Critical angle θ_c and frequency f evolutions versus grid number of points for $L_z = 0.8$ (θ_c values are obtained by linear interpolation)

$(n_x \times n_y \times n_z)$	θ_c (°)	f (Hz)
$300 \times 150 \times 40$	30.97°	763.7
$300 \times 150 \times 50$	31.12°	720.1
$300 \times 180 \times 50$	31.48°	705.3
$400 \times 180 \times 50$	31.71°	700.4
$400 \times 180 \times 60$	31.83°	700.0
$400 \times 200 \times 50$	31.78°	700.1
$400 \times 220 \times 50$	31.82°	700.1
$500 \times 180 \times 50$	31.79°	700.2
$600 \times 200 \times 50$	31.83°	699.8

5.2.3 3D unsteady behavior

When the incident shock angle and the spanwise length are equal to $\theta = 32°$ and $L_z = 0.8$, respectively, the flow is 3D and unsteady. However the onset of the unsteadiness is not a direct scenario. Figure 11 shows the time evolution of the physical residual based on the conservative ρW variable (the CPU time figures in the second x-axis). The monotonous unsteady state is reached after several characteristic stages that can be connected with different instabilities. Surface streamlines and 3D views are presented in Figs. 12 and 13 for different moments (from A to F). During the first stage (from A to B) from $t = 0$ to $t = 16$ ms, the flow remains 2D and stationary. State A corresponds to the initial state of the computation which is not solution of the 3D

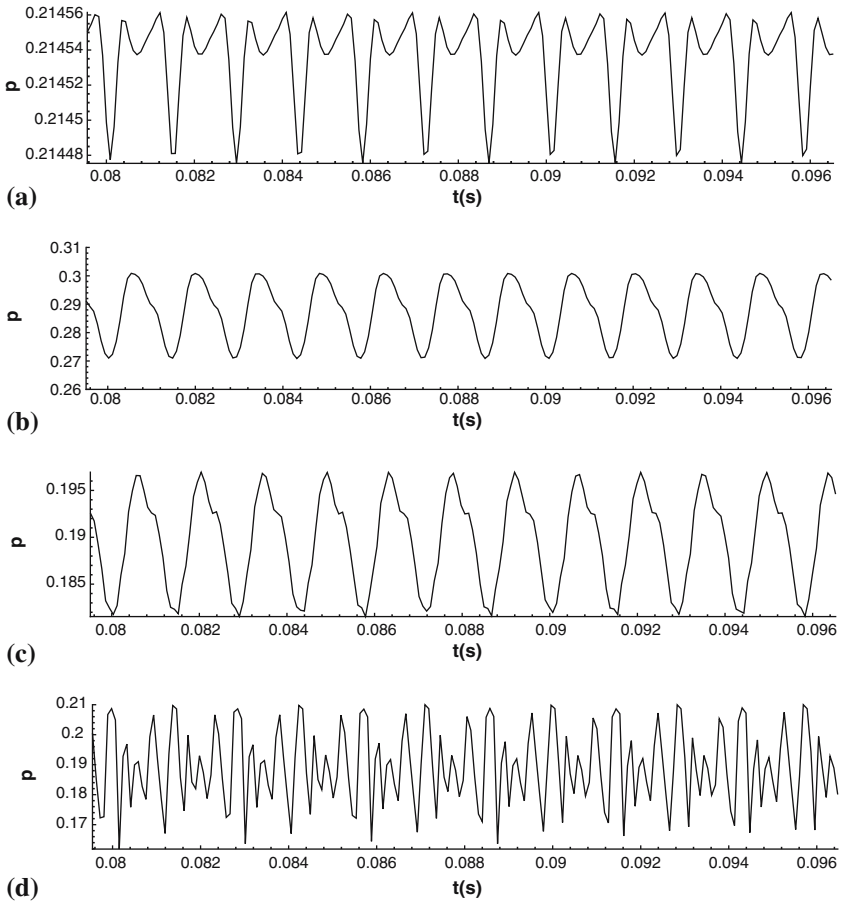

Fig. 9 Temporal pressure evolution for different points in the flow. **a** $(x_0, y_0, z_0) = (0.8053, 0.6, 0.4)$, **b** $(0.8053, 0.28, 0.4)$, **c** $(0.8053, 0.18, 0.4)$ and **d** $(0.8053, 0.042, 0.4)$ for $\theta = 32.5°$ and $L_z = 0.8$

equations. The state B is solution to the 3D equations and it is corresponds to 2D flow which is very close to the solution obtained by 2D Navier–Stokes equations. After this state, a first bifurcation appears in the residual evolution. A 3D instabilities is observed with transverse wavelength close to 0.4 while the z-dimension L_z is 0.8 (from B to C). Four counter rotating vortex tubes similar to those described in the previous paragraph appear. From $t = 35$ ms a second instability appears but with a transverse wavelength close to 0.7 (from C to D). At this time, two instabilities are simultaneously present with different wavelengths, 0.4 and 0.7. From $t = 44$ ms, the instability with the shortest wavelength disappears (from D to E). The residual decreases then of two orders up until $t = 58$ ms when a Hopf bifurcation (characterized in previous section) leads the flow toward an unsteady state (F). A FFT on the temporal pressure evolution permits to extract the main frequency (Fig. 10). The fundamental frequency is close to 700 Hz and this frequency is in evidence in all flow. The secondary frequencies correspond to the harmonics of this fundamental frequency. Inside the bubble, Figs. 9d and 10d, a sub-harmonic frequency (350 Hz) and a broadband frequency around 3,000 Hz are also observed. In last characteristic is a purely local and only observable inside the bubble. The main unsteady dynamics (700 Hz) is related to a breathing of the bulb which is connected to 3D movement with an important transverse (z) component. The size and shape evolution of the bulb is presented in Fig. 14. Other simulations were carried out for a transverse length L_z equal to 1 where the temporal residual evolution shows a similar process passing by intermediate unstable 3D states with different wavelengths which interact for finally reaching a stable 3D and unsteady state. Figure 14 shows this residual evolution. When L_z becomes large, a privileged wavelength of instabilities exists. Indeed, when $L_z = 2$ or 3 the wavelength obtained when t is large does not change and it is equal to $\lambda_z \sim 0.7$. Fig. 15 shows the streamline surface for $L_z = 2$ and $\theta = 32°$ and the z-component of the friction coefficient on the plate is shown on the fig. 16 for two L_z values (2 and 3). In these two cases, the final wavelength is close to 0.7.

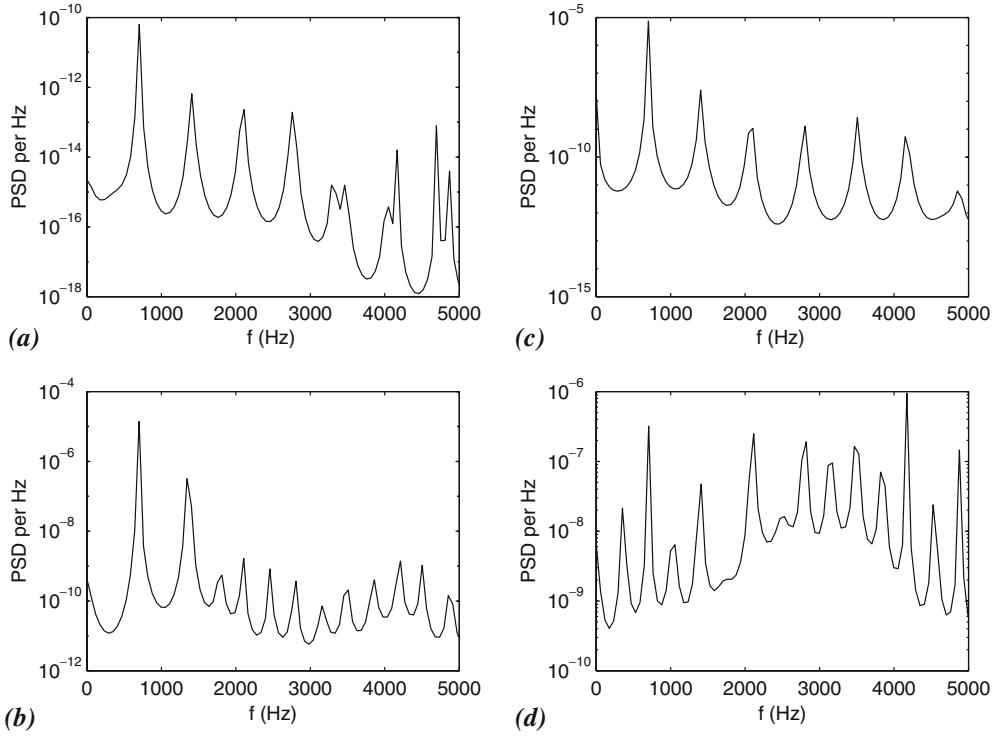

Fig. 10 Pressure spectra density for different points in the flow. **a** $(x_0, y_0, z_0) = (0.8053, 0.6, 0.4)$, **b** $(0.8053, 0.28, 0.4)$, **c** $(0.8053, 0.18, 0.4)$ and **d** $(0.8053, 0.042, 0.4)$ for $\theta = 32.5°$ and $L_z = 0.8$

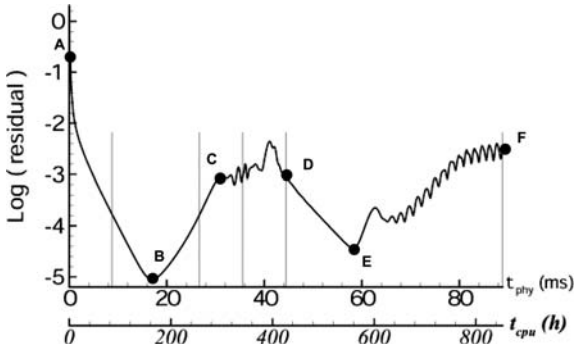

Fig. 11 Residual time evolution and CPU time on a 2.4 GHz Pentium processor, $L_z = 0.8$, $\theta = 32°$.

6 Scenario and conjecture

This study has shown that self-sustained low frequency oscillations can appear in a strictly laminar SWBLI without upstream perturbations. This destabilizing process of a SWBLI seems to lead to complex scenario where the flow is a 3D and unsteady nonlinear state with the transverse structuring of the flow is the same order of magnitude as the size of the separated zone. This behavior is compatible with the work of Theofilis et al. [23] on the existence of a 3D and stationary global mode in separated boundary layer. However this work is limited to the incompressible and linear theory framework. Moreover, Theofilis suggests that this stationary 3D global mode is a precursory sign of the "vortex shedding" phenomenon. In an incompressible regime, this scenario was confirmed by experimental observations carried out by Dallmann [24] and Dallmann et al. [25].

The results presented in the previous sections seem to suggest that in a SWBLI this scenario can also be applied under given assumptions. Indeed, when the incident shock angle is not too high $\theta \leq 32.5°$, there are some bifurcations modifying the flow from a stationary 2D flow configuration to an unsteady 3D one. These different processes are synthesized on Fig. 17. These results highlight, when $\theta < 31.7°$, that the flow

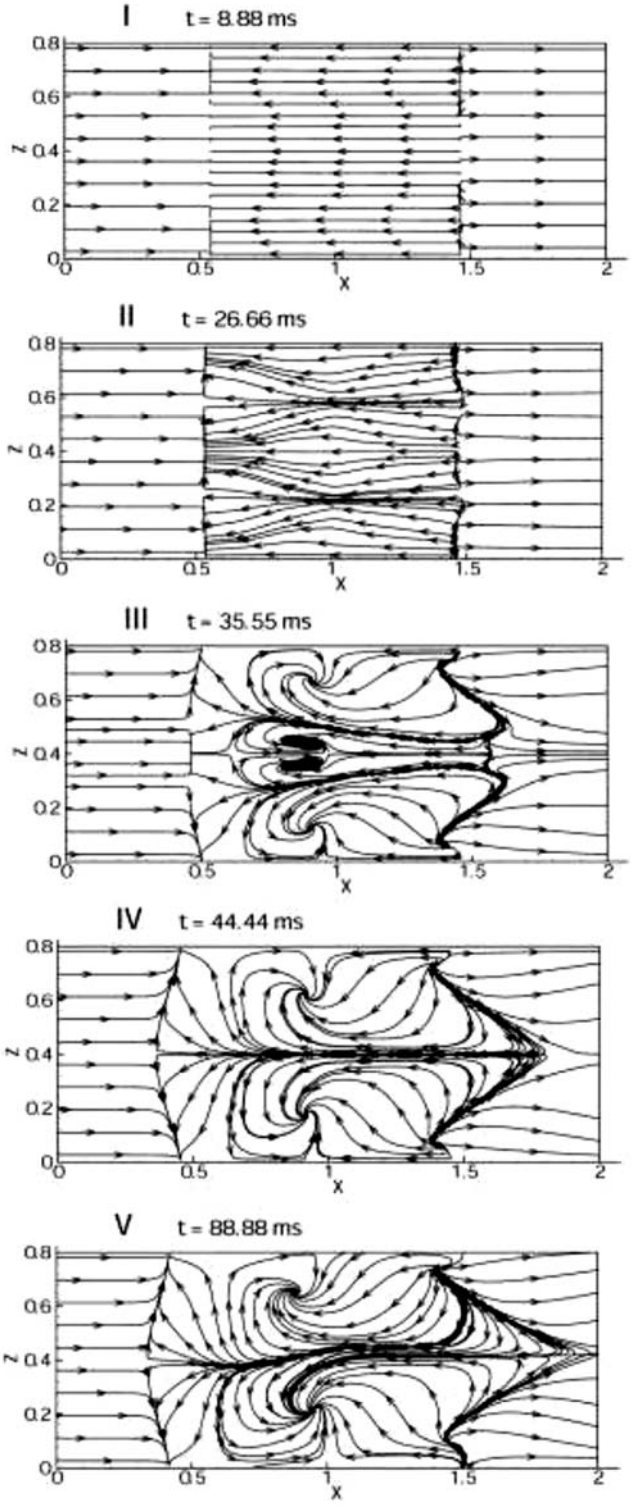

Fig. 12 Surface streamlines on the plate at different moments, $L_z = 0.8$, $\theta = 32°$

is globally stable $\forall L_z$ (if the purely convective instabilities are not taken into account). For these values of θ, the flow is 2D and stationary. For an unlimited flow in z direction and when $\theta > 31.7°$, the flow is unstable and bifurcate from a stationary 2D flow to an unsteady 3D flow. More precisely, it would seem that the flow

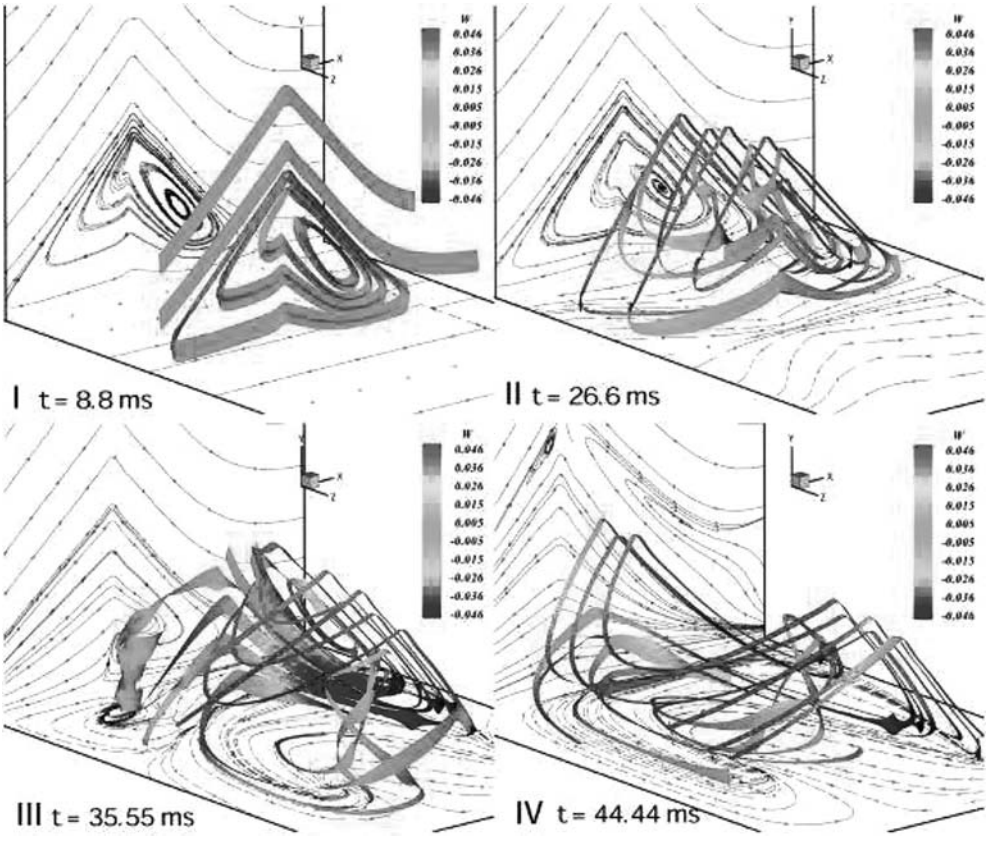

Fig. 13 3-Dimensional views inside the bulb at different moments, $L_z = 0.8$, $\theta = 32°$

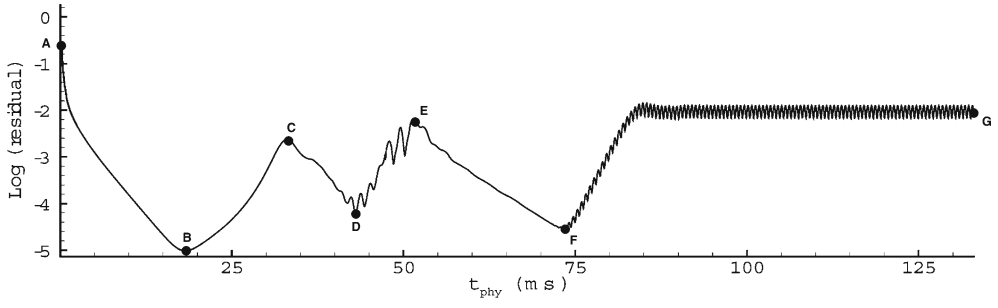

Fig. 14 Residual time evolution and CPU time on a 2.4 GHz Pentium processor for $L_z = 1$, $\theta = 32°$

bifurcates initially towards a stationary 3D flow but this flow regime is again unstable and then bifurcates towards an unsteady 3D flow. This assumption was confirmed by a BiGlobal linear stability analysis and will be presented in a future paper. When transverse dimension is limited $L_z < 0.8$, it is possible to isolate a zone where the flow is 3D stationary and remains stable. This zone of stability tends to decrease when the angle increases.

Considering these results we can thus conjecture the following scenario: when a separation reaches a critical size (clearly not quantified in our calculations), it becomes unstable, 3D and stationary. This 3D process can be rather complex by the existence of several wavelengths in the transitional stage. The origin of this 3D characteristic could be, as suggested by Theofilis, the existence of a global instability with a wavelength that would be lower than 0.8 times of X_{sh}, the interaction length. However, it would seem that this flow can be

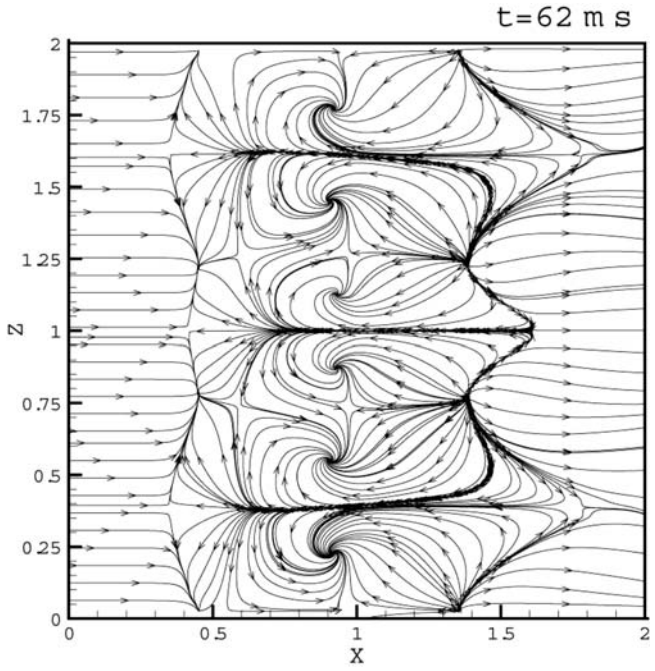

Fig. 15 Surface streamlines on the plate at t = 62 ms, $\theta = 32°$, $L_z = 2$

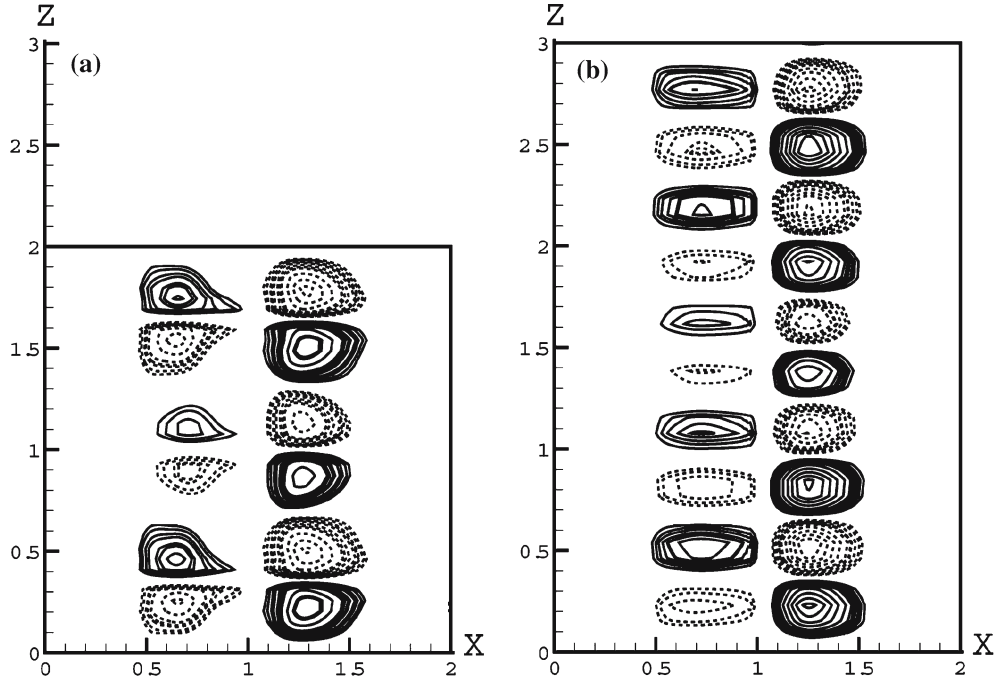

Fig. 16 z-Component of the friction coefficient on the plate, $\theta = 32°$, $L_z = 2$ **(a)**, $L_z = 3$ **(b)**

again unstable and finally leads to 3D unsteady configuration. The whole process that leads to a 3D unsteady flow seems to be faster when the incident shock angle is large or if the Reynolds is high (not shown here). In all our numerical simulations, the resulting unsteady dynamics corresponds to a low frequency breathing of the separated zone without convected structure (no vortex shedding and no breaking bubble were observed). However the breathing of the bulb should be confirmed by further study when the convective instabilities are computed. Indeed, as it was indicated throughout the article, different convective instabilities, in particular the Kelvin–Helmholtz instability in the vicinity of the shear layer in the separated zone, are not taken into account.

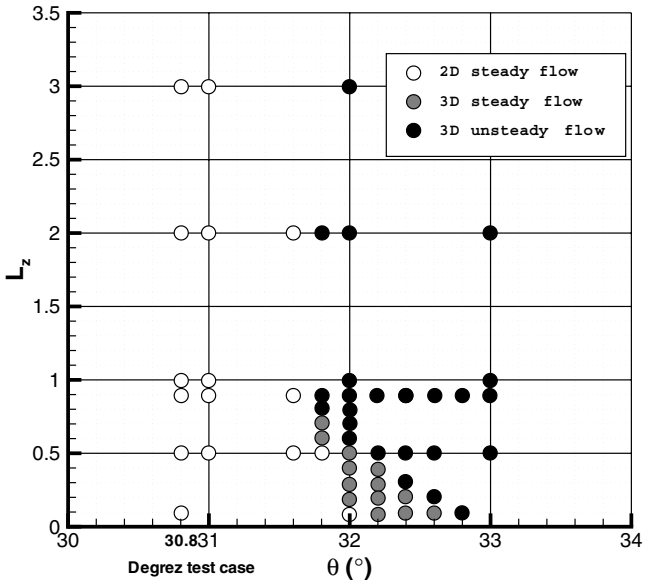

Fig. 17 Flow organization according to the incident shock angle and the transverse size of the computation domain

These instabilities can play an important role in unsteady dynamics even if they have a general characteristic frequency of at least a higher magnitude order ($\sim$ kHz) than the frequencies observed in the breathing of the bulb. Indeed, the interaction between these convective instabilities and the global instabilities inside the bulb could generate a rupture of the separated zone and consequently the creation of vortex shedding as the several experimental results seem to suggest it (Dupont et al. [26]). In addition, this process seems relatively robust to be able to exist in a fully turbulent SWBLI.

7 Conclusions and prospects

The main objective of this study was to show that a laminar SWBLI could, under some assumptions, be the place of unsteady self-sustained low frequency dynamics. Therefore, 2D and 3D numerical simulations were carried out for a configuration close to the Degrez et al. where the incident shock angle is gradually increased.

These numerical simulations highlighted a complex process in the onset of unsteady dynamics when the angle of the incident shock increases. Indeed, 3D calculations have shown that before becoming unsteady, the SWBLI goes through a phase where the flow becomes 3D and stationary (for $\theta > 31.7°$). However, this state is unstable and can lead to a fully 3D and unsteady flow. The final state is reached all the more quickly as the angle of the incident shock is large.

When transverse dimension L_z is large enough, the principal transverse wavelength of flow is close to $\lambda_z = 0.7$. In the interaction, the bulb topology is complex and mainly characterized by cells in transverse direction where the flow is alternatively separated and reattached. Within this separated zone, the flow can be complex like vortex waterspout which connect the flow from the wall to the downstream shear layer of the interaction.

This study has shown that the unsteady self-sustained low frequency dynamics (here $f \simeq 700$ Hz) in SWBLI is not directly connected to the turbulent state of the flow. Moreover, these results show that it is not necessary to have upstream disturbances of the interaction to generate a self-sustained oscillation of SWBLI. However, the existence of upstream disturbances related to the turbulent character of the boundary layer or related to mechanisms of instability involving in the transition process have a great influence on the unsteady dynamics of the interaction. It would be interesting to verify if the results presented in this paper remain unchanged when there are disturbances in of upstream the interaction. The principal difficulty is to extract both the Kelvin–Helmholtz instabilities and the global dynamics that are characterized by very different temporal and spatial range scales ($t_{KH} \sim 5 \times 10^{-5}$ s and $\lambda_{KH} \sim \delta$ (δ: boundary layer scale), $t_G \sim 10^{-3}$ s and $\lambda_G \sim X_{sh}$).

At this stage no distinction have been done between the bulb dynamic and the reflected shock one but it seems, as shown experimentally by Dupont et al. [27] and Haddad et al. [28], that the reflected shock has its own strong low frequency dynamics on the root of the shock. Thus, it would be interesting to study a more intense SWBLI where the reflected shock is fully developed as it can be observed in a fully turbulent flow. At the same time, a study on a compressible separated boundary layer without incident shock should permit better understanding of the dynamic of the bulb alone.

Acknowledgements Computing time was provided by Institut du Développement et des Ressources en Informatique Scientifique (IDRIS)-CNRS.

References

1. Lighthill, M.J.: Reflection at a laminar boundary-layer of a weak steady disturbance to a supersonic stream neglecting viscosity and heat conduction. Q J. Mech. Appl. Math. **3**, 303 (1950)
2. Lighthill, M.J.: On the boundary layer upstream influence ii supersonic flows without separation. Proc R Soc A **217**, 478–507 (1953)
3. Ribner, H.S.: Convection of pattern of vorticity through a shock wave. 2: Technical report, NASA 1953
4. Kovasznay, L.S.G.: Turbulence in supersonic flow. J. Aero Sci. **20**, 657–682 (1953)
5. Morkovin, M.V.: Effects of compressibility on turbulent flows. In: International symposium. on the Mécanique de la turbulence, Paris France, pp. 367–380 1962
6. Debiève, J.F., Lacharme, J.P.: A shock-wave/free turbulence interaction. Turbulent shear layer/shock wave interaction, IUTAM symposium Palaiseau, pp. 392–403 (1985)
7. Green, J.E.: Reflexion of an oblique shock wave by a turbulent boundary layer. J. Fluid Mech. **40**, 81–95 (1970)
8. Dolling, D.S.: Fifty years of shock-wave/boundary-layer interaction research: what next? AIAA J. **39**, 8 (2001)
9. Smits, A.J., Muck, K.C.: Experimental study of three shock wave/turbulent boundary layer interactions. J. Fluid Mech. **182**, 291–314 (1987)
10. Plotkin, K.J.: Shock wave oscillation driven by turbulent boundary-layer fluctuations. AIAA J. **13**, 1036–1040 (1975)
11. Thomas, F.O., Putnam, C.M., Chu, H.C.: On the mechanism of unsteady shock oscillation in shock wave/turbulent boundary layer interactions. Exp. Fluids **18**, 69–81 (1994)
12. Dolling, D.S., Or, C.T.: Unsteadiness of the shock wave structure in attached and separated compression ramp flow. Exp. Fluids **3**, 24–32 (1985)
13. Selig, M.S., Smits, A.J.: Effect of periodic blowing on attached and separated supersonic turbulent boundary layer. AIAA J. **29**, 1651–1658 (1991)
14. Degrez, G., Boccadoro, C.H., Wendt, J.F.: The interaction of an oblique shock wave with a laminar boundary layer revisited. an experimental and numerical study. J. Fluid Mech. **177**, 247–263 (1987)
15. Liou, M.S., Edwards, J.: Low-diffusion flux-splitting methods for flows at all speeds. AIAA J. **36**, 1610–1617 (1998)
16. Alfano, D., Corre, C., de la Motte, J., Lerat, A.: Assesment of numerical methods for unsteady shock/boundary layer interaction. Boundary and interior layers – computational and asymptotic methods BAIL 2004) conference, Toulouse, Juillet 2004
17. Kim, K.H., Kim, C., Rho, O.-H.: Methods for the accurate computations of hypersonic flows i. ausmpw+ scheme. J. Comput. Phys. **174**, 38–80 (2001)
18. Kim, K.H., Kim, C., Rho, O.-H.: Methods for the accurate computations of hypersonic flows ii. shock-aligned grid technique. J Comput Phys **174**, 81–119 (2001)
19. Peyret, R., Taylor, T.: Computational methods for fluid flows. Berlin Heidelberg New York: Springer 1983
20. Jameson, A.: Time-dependent calculations using multigrid with applications to unsteady flows past airfoils and wings. AIAA Paper 1991
21. Luo, H., Baum, J.D., Lhner, R.: An accurate, fast, matrix-free implicit method for computing unsteady flows on unstructured grids. Comput. Fluids **30**, 137–159 (2001)
22. Robinet, J.-Ch., Daru, V., Tenaud, Ch.: Two-dimensional laminar shock wave/boundary layer interaction. In: BAIL conference, Toulouse France 2004
23. Theofilis, V., Hein, S., Dallmann, U.: On the origin of unsteadiness and three-dimensionality in a laminar separation bubble. Phil. Trans. R. Lond. A **358**, 3229–3246 (2000)
24. Dallmann, U.: Three-dimensional vortex structures and vorticity topology. In: IUTAM symposium on fundamental aspects of vortex motion, Tokyo Japan 1988
25. Dallmann, U., Herberg, H., Gebing, H., Su, W.-H.: Flow field diagnostics: topological flow changes and spatio-temporal flow structures. AIAA Paper 95-0791 1995
26. Dupont, P., Debiève, J.F., Haddad, C., Dussauge, J.P.: Three-dimensional organization and unsteadiness of a shock wave/turbulent boundary layer interaction. ISSW-04, Sendai Japan 2004
27. Dupont, P., Debiève, J.F., Ardissone, J.P., Haddad, C.: Some time properties in shock boundary layer interaction. West East High Speed Fields, CIMNE, Barcelona Spain 2002
28. Haddad, C., Ardissone, J.P., Dupont, P., Debiève, J.F.: Space and time organization of a shock wave/turbulent boundary layer interaction. Congrès AAAF, Aérodynamiques instationnaires, Paris 2004